The fungal microbiota modulate neonatal oxygen-induced lung injury

Isaac Martin, Mary Silverberg, Ahmed Abdelgawad, Kosuke Tanaka, Brian A. Halloran, Teodora Nicola, Erin D. Myers, Jay P. Desai, Catrina T. White, Ibrahim Karabayir, Oguz Akbilgic, Laura Tipton, Samuel J. Gentle, Namasivayam Ambalavanan, Brian M. Peters, Viral G. Jain, Luan D. Vu, Charitharth V. Lal, Stephania A. Cormier, Joseph F. Pierre, Tamás Jilling, Ajay J. Talati, and Kent A. Willis

ONLINE DATA SUPPLEMENT

Key Resource Table

Reagent	Company - Catalog #	RRID
Teklad S-2335 Mouse Breeder Sterilizable Diet	Envigo - 7904.15	
Penicillin VK	Thermo Fisher Scientific (TFS)- AC455230050	
Cefoperazone Sodium	TFS - AAJ6518506	
Clindamycin Sodium	TFS - 1G 11-101-3689	
Polyethylene glycol 3350 (Miralax)	TFS - J61495.AK	
Ertapenem Sodium	Fisher - 50-997-777 5G	
Vancomycin HCL	Milipore Sigma - 1404-93-9	
Neomycin Sodium	TFS - 50-186-3466	
Fecal Microbiota Transplant	This study only	
Lamina Propria Isolation Kit, Mouse	Miltenyi Biotec - 130-097-410	
Hank's Balanced Salt Solution	TFS - 14170112 or 14025092	
DNase I	Sigma - D5025	
Collagenase, Type I	Invitrogen - 7100017	
Fetal Bovine Serum	Millipore Sigma - F2442-500ML	
C-Tube	Miltenyi Biotec - 130-096-334	
RBC lysis buffer	Biolegend - 420301	
IC Fixation Buffer	TFS - 00-8222-49	

Permeabilization Buffer	TFS - 00-8333-56	
VMR Cell Strainers, 40, 70 µm	Avantor - 76327-098	
V-bottom, 96 well plate	Greiner Bio-One - 651901	
Sabouraud Dextrose Broth 4% (pH 5.6)	TFS - R064416	
zymoBIOMICS microbial community standards	Zymo Research - D6300 and D6310	
zymoBIOMICS microbial community DNA standards	Zymo Research - D6305/6306 and D6311	
zymoBIOMICS spike-in control I	Zymo Research - D6320-10	
zymoBIOMICS spike-in control II	Zymo Research - D6321-10	
zymoBIOMICS gut microbiome standard	Zymo Research - D6331	
RNase-free DNase Set	Qiagen - 79254	
QIAshredder	Qiagen - 79656	
PrimeScript RT Master Mix	Takara Biosciences - RR036B	
Bioanalyzer High Sensitivity DNA Analysis Kit	Agilent Technologies - 5067-4626	
Paraformaldehyde, 4% w/v aq. soln.	TFS - 047392.9M	
Antigen Retrieval Buffer	Abcam - ab93678	
ProLong Diamond Anti-Fade Mounting Media with DAPI	TFS - P36962	RRID:AB_2307445
ArC™ Amine Reactive Compensation Bead Kit	Invitrogen - A10346	

UltraComp eBeads	Invitrogen - 01-2222-41	
Antibodies		
Ghost Dye Violet 510	TonboBio - 13-0870-T100	
LIVE/DEAD Fixable Blue Dead Cell Stain Kit, for UV removal	Invitrogen - L23105	
Mouse BD Fc Block (CD16/32)	BD Biosciences - 553142	RRID:AB_394656
Ly-6-G Pacific Blue™	Biolegend - 127611	RRID:AB_1877212
MERTK (Mer) BV 711	Biolegend - 151515	RRID:AB_2876505
CD64 (FcγRI) FITC	Biolegend - 139315	RRID:AB_2566555
F4/80 BUV737	BD Biosciences - 749283	RRID:AB_2873658
Ly-6C Brilliant Violet 605™	Biolegend - 128035	RRID:AB_2562352
CD11c - BV650	Biolegend - 117339	RRID:AB_2562414
CD169 (Siglec-1) APC	Biolegend - 142417	RRID:AB_2565640
CX3CR1 Recombinant PE	Biolegend - 153705	RRID:AB_2734221
CD170 (Siglec-F) - BV421	Biolegend - 155509	RRID:AB_2810421
CD3ε (17A2) violetFluor™ 450	TonboBio - 75-0032	RRID:AB_2621923
CD3ε BUV 737	BD - 612771	RRID:AB_2870100
CD19 Pacific Blue™	Biolegend - 115526	RRID:AB_493341
CD11b Pacific Blue™	Biolegend - 101224	RRID:AB_755986
CD49b (pan-NK cells) Pacific Blue™	Biolegend - 108918	RRID:AB_2265144
F4/80 Pacific Blue™	Biolegend - 123123	RRID:AB_893487
FcεRIα Pacific Blue™	Biolegend - 134313	RRID:AB_10612933
CD90.2 (Thy1.2) FITC	Biolegend - 105306	RRID:AB_313177

CD127 (IL-7Rα) APC	Biolegend - 135012	RRID:AB_1937216
CD45 APC/Cyanine7	Biolegend - 103116	RRID:AB_312981
IL-33R (ST2) (RMST2-33), PE	TFS - 12-9333-82	RRID:AB_2572706
RORγt, PerCP-Cy™5.5	BD Biosciences - 562683	RRID:AB_2737720
GATA3, PE-Cy™7	BD Biosciences - 560405	RRID:AB_1645544
αSMA Monoclonal Anti-mouse, IgG	Abcam - ab7817	RRID:AB_262054
von Willebrand Factor (vWF), Polyclonal Rabbit Anti-mouse, IgG	TFS, Invitrogen - PA5-16634	RRID:AB_10982615
CD169 (Siglec1), Clone 3D6.112, Monoclonal Rabbit Anti-mouse, IgG	Novus Biologicals - NBP3-08989-0.1mg	RRID:AB_2923219
CD11c Monoclonal Armenian Hamster Anti-mouse, IgG	TFS, Invitrogen - 14-0114-82	RRID:AB_467115
F4/80 Purified anti-mouse Antibody	Biolegend - 123102	RRID:AB_893506
Alexa Fluor™ 488 Tyramide SuperBoost™ Kit, goat anti-rabbit IgG	TFS - B40922	
Alexa Fluor™ 647 Tyramide SuperBoost™ Kit, goat anti-mouse IgG	TFS - B40916	
Goat anti-Hamster IgG (H+L) Cross-Adsorbed Secondary Antibody, Alexa Fluor™ 647	TFS, Invitrogen - A-21451	RRID:AB_2535868
Goat anti-Rat IgG - Alexa Fluor™ 555	Invitrogen - A-21434	RRID:AB_2535855
Chicken anti-Mouse IgG - AF™	Invitrogen- A-21463	RRID:AB_2535869

647		
Goat anti-Rabbit IgG - AF™ 555	Invitrogen- A-21428	RRID:AB_2535849
Goat anti-Hamster IgG (H+L) Cross-Adsorbed Secondary Antibody, Alexa Fluor™ 647	TFS, Invitrogen - A-21451	RRID:AB_2535868
Goat anti-rabbit-HRP antibody	Cell Signaling - 7074	RRID:AB_2099233
Donkey anti-goat-HRP antibody	SouthernBiotech - 6402	RRID:AB_2796335
Primer Sequences		
Bacterial 16S, V4-V5, 450 bp	515F	GTGCCAGCGCCGCGGTAA
	907R	CCGTCAATTCCTTTGAGTTT
Fungal, ITS1, 200-400 bp	ITS5-1737F	GGAAGTAAAAGTCGTAACAAGG
	ITS2-2043R	GCTGCGTTCTTCATCGATGC
Fungal, ITS2, 380 bp	ITS3-2024F	GCATCGATGAAGAACGCAGC
	ITS4-2409R	TCCTCCGCTTATTGATATGCTCCTCCGCTTATTGATATGC
Organisms		
C57Bl/6J mouse	Jackson Laboratory - 000664	RRID:IMSR_JAX:000664
Equipment		
Luminex 200 System	Merck Millipore	RRID:SCR_018025
ProOx 360 controller	BioSpherix	RRID:SCR_021130
gentleMACS	Miltenyi Biotec	RRID:SCR_020271

FACS Symphony A5 SE	BD Biosciences	RRID:SCR_022674
A1R HD confocal microscope	Nikon	RRID:SCR_020317
flexiVent	SCIREQ	RRID:SCR_022673
Vevo 770 High-Resolution *in vivo* Micro-Imaging System	Fujifilm VisualSonics	RRID:SCR_022921
2100 Bioanalyzer Instrument	Agilent	RRID:SCR_018043
QuantStudio 6	Applied Biosciences	RRID:SCR_020239
Rotor-Gene Q Series	Qiagen	RRID:SCR_018976
NovoSeq 6000 system	Illumina	RRID:SCR_016387
MiSeq platform	Illumina	RRID:SCR_020133
HiSeq 4000 platform	Illumina	RRID:SCR_016386
Software		
NICHD Neonatal Outcomes Estimator	https://neonatal.rti.org	
FACSDiva	BD Biosciences - v9.0	RRID:SCR_001456
FlowJo for Mac	BD Biosciences - v10.8.1	RRID:SCR_008520
Rotor-Gene Q Series Software	Qiagen	RRID:SCR_015740
FIJI	https://fiji.sc	RRID:SCR_002285
Prism 10 for Mac	GraphPad - v10.2.3	RRID:SCR_002798
SPSS Statistics	IBM - 28.0.1	RRID:SCR_002865
R	R project for statistical computing - 4.2.2	RRID:SCR_001905
RStudio	Posit - 2022.12.0	RRID:SCR_000432
phyloseq	1.42.0	RRID:SCR_013080
vegan	2.6-4	RRID:SCR_011950

DESeq2	v1.38.2	RRID:SCR_015687
mia	1.6.0	RRID:SCR_023619
SpiecEasi	1.1.2	RRID:SCR_022712
igraph	1.4.1	RRID:SCR_019225
caret	6.0-94	RRID:SCR_021138
QIIME 2	2022.11	RRID:SCR_021258
DADA2	v1.26	RRID:SCR_023519
PERFect	0.2.4	RRID:SCR_024682
SILVA	138.1	RRID:SCR_006423
UNITE	9.0	RRID:SCR_006518
NCBI MOLE-BLAST		RRID:SCR_004870
CLC Genomic Workbench	Qiagen - v22	RRID:SCR_011853
ClustVis	https://biit.cs.ut.ee/clustvis/	RRID:SCR_017133
Ingenuity Pathway Analysis	Qiagen (July 2022 edition)	RRID:SCR_008653
Datasets		
RNAseq, Mouse	This paper	PRJNA982880
16S, human	This paper	PRJNA982880
16S, mouse	This paper	PRJNA982880
ITS2, human	This paper	PRJNA982880
ITS2, mouse	This paper	PRJNA982880

Resource Availability

Lead Contact: Further information and requests for resources and reagents should be directed to and will be fulfilled by the lead contact, Kent Willis (kawillis@uab.edu).

Materials Availability: This study did not generate unique reagents or transgenic animals.

Data Availability:

- Raw RNA-seq, 16S, and ITS2 sequencing data are deposited at the NCBI Sequence Read Archive (Access Number: PRJNA982880).
- Processed data files and original code are available at github.com/WillisLungLab/MiBPD.
- Any additional data required to reanalyze the data presented in this paper are available from the lead contact upon request.

Supplemental Information

The fungal microbiota predicts BPD development:
To test the predictive potential of the mycobiota, we first developed random forest machine-learning models using fungal or bacterial microbiomes as exploratory analyses (supplemental figure S4). The fungal model (supplemental figure S4a-b), which had an area under the receiver operating curve of 0.74, identified several rare fungal phyla, such as *Mucoromycota, Mortierellomycota, and Rozellomycota ,* as the most discriminatory taxa. In the bacterial model, which had a receiver operating curve of only 0.48, *Actinobacteriota and Bacteroidota* were the most discriminatory taxa (supplemental figure S4c-d).

Distinct fungal community clusters are linked to clinical outcomes**:**
Having shown that fungal microbiota features are associated with BPD development, we sought to identify other clinical characteristics that may contribute to heterogeneity in the composition of the neonatal mycobiome. First, we used PERMANOVA to screen potential additional contributors to fungal community composition. None of the potential fungal microbiome covariates we examined remained significant after adjustment for false discovery (supplemental table S3, figure S7). We made similar observations when we tested potential bacterial covariates (supplemental table S4).

Bacterial DMM models:
DMM modeling using the bacterial microbiome data is shown in supplemental figures S8 and S9. Laplace clustering for the whole microbiome indicated optimal clustering with 4 clusters (supplemental figure S9a), while clustering for the NoBPD and BPD infants was optimal with 2 clusters each (supplemental figures S9d and g). We then performed variable importance analysis and identified bacterial ASVs with significant contributions to component formation (supplemental figure S9). Clustering in the whole microbiome model is driven by *Enterococcus*, *Enterobacter*, *Cellulosimicrobium*,

Escherichia-Shigella, and multiple *Klebsiella* ASVs. Clustering in NoBPD infants was driven by *Enterococcus, Staphylococcus,* and multiple *Klebsiella* FASVs, while *Enterococcus, Enterobacter,* and *Klebsiella* ASVs drove the BPD infant clusters. CCA showed Cluster 2 of the overall bacterial model was associated with BPD, critical illness, AMAB, and positive CRP (supplemental figure S9c). Together, the DMM clustering between the fungal and multikingdom microbiome models is not indicative of any significant overlap.

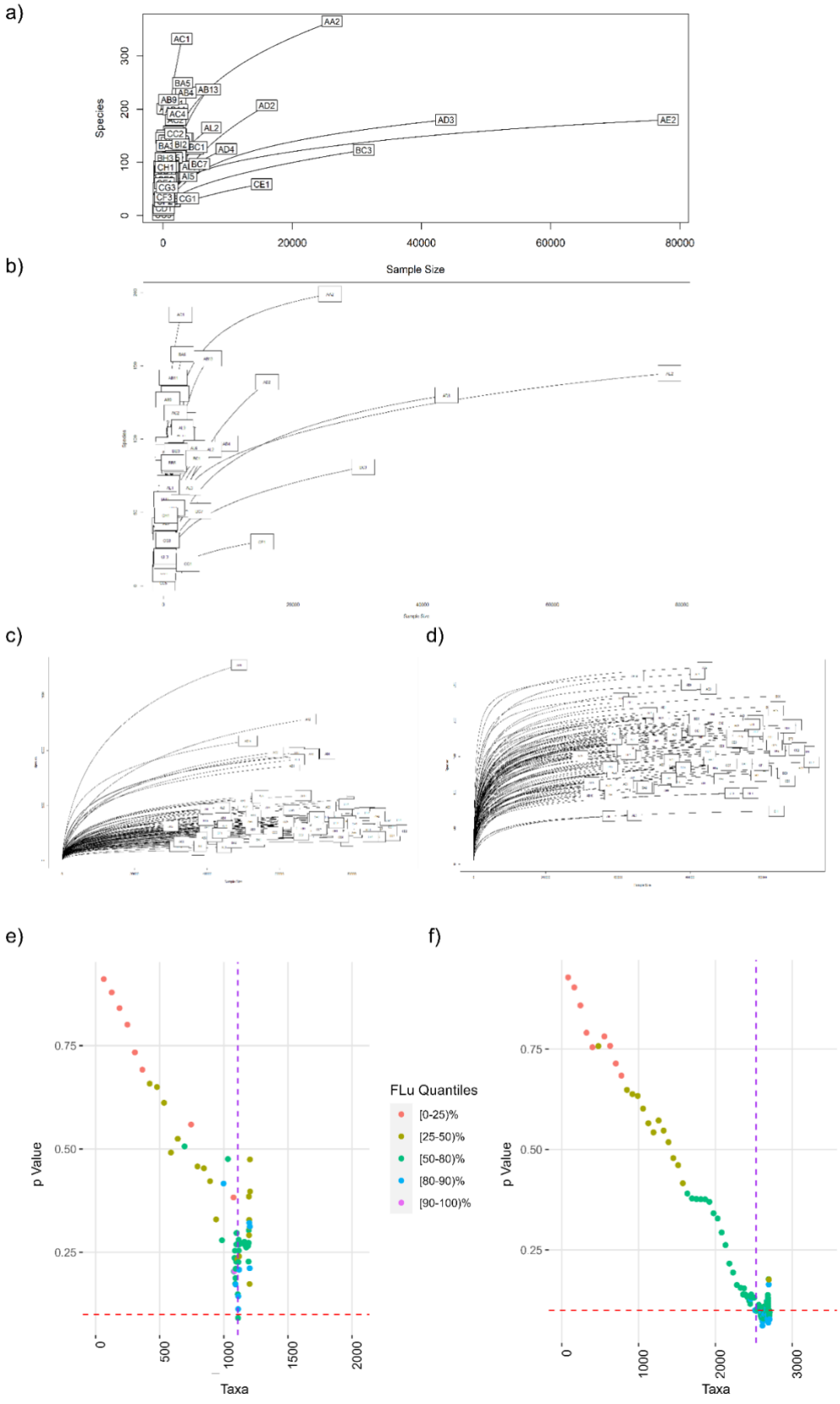
a)
b)
c)
d)
e)
f)
Species
Sample Size
AA2
AC1
BA5
AB13
AB9
AC4
AD2
AL2
AD3
AE2
CC2
BC1
AD4
BC3
CH1
ABC7
AI5
CG3
CE1
CF3
CG1
0
20000
40000
60000
80000
100
200
300
p Value
Taxa
FLu Quantiles
[0-25)%
[25-50)%
[50-80)%
[80-90)%
[90-100)%
0.25
0.50
0.75
500
1000
1500
2000
3000

Figure S1. Source contamination modeling. a) Rarefication plot of unfiltered ITS2 sequencing. b) Rarefication plot of ITS2 sequencing after decontamination modeling with PERFect. c) Rarefication plot of unfiltered 16S sequencing. d) Rarefication plot of 16S sequencing after decontamination modeling with PERFect. e) Fungal taxa filtering loss plots. f) Bacterial taxa filtering loss plots. Please see tables of filtered taxa at github.com/WillisLungLab/MiBPD/SourceContamination.

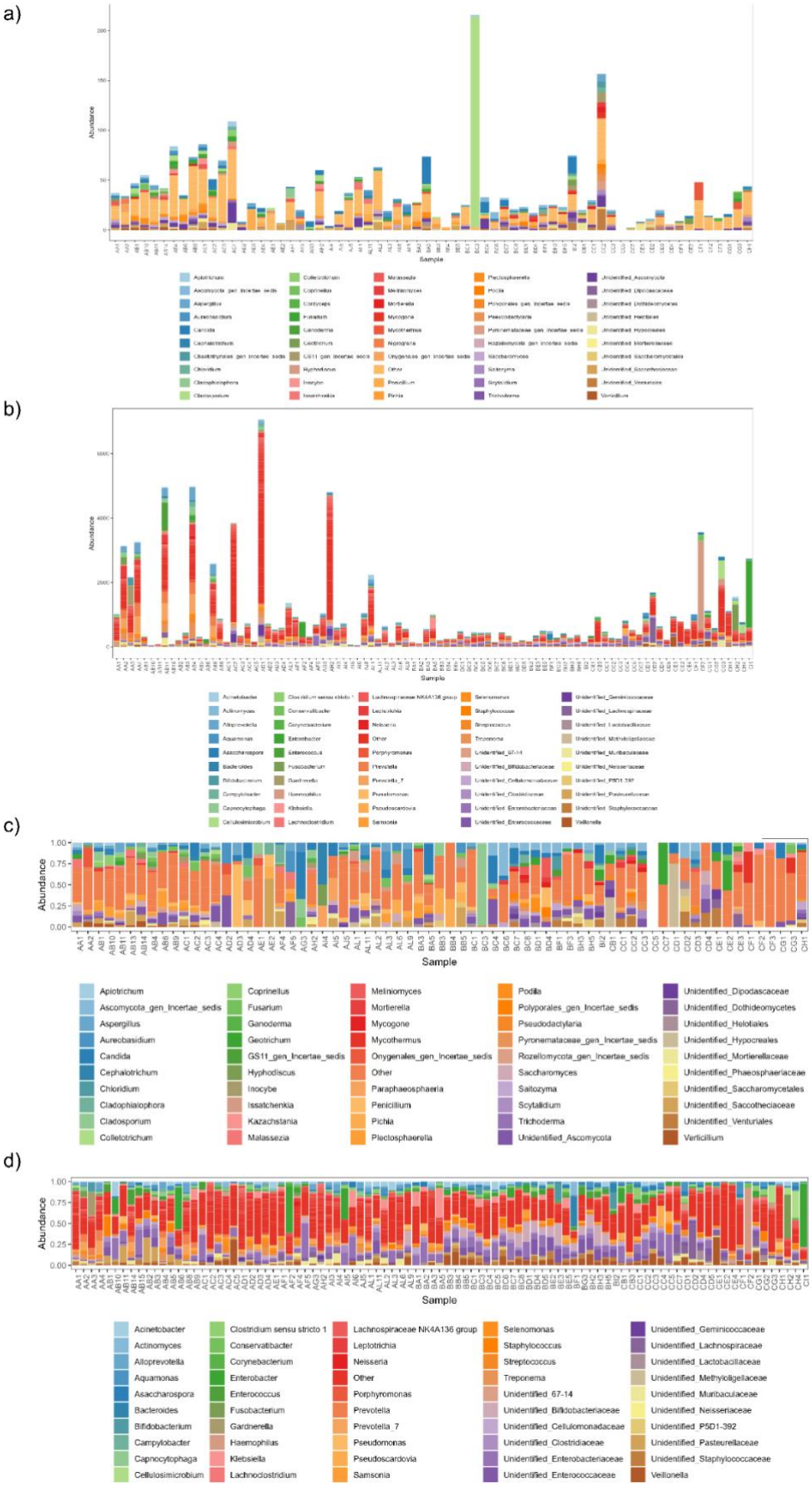
a)
b)
c)
d)
Abundance
Sample
Apiotrichum
Ascomycota_gen_Incertae_sedis
Aspergillus
Aureobasidium
Candida
Cephalotrichum
Chloridium
Cladophialophora
Cladosporium
Colletotrichum
Coprinellus
Fusarium
Ganoderma
Geotrichum
GS11_gen_Incertae_sedis
Hyphodiscus
Inocybe
Issatchenkia
Kazachstania
Malassezia
Meliniomyces
Mortierella
Mycogone
Mycothermus
Onygenales_gen_Incertae_sedis
Other
Paraphaeosphaeria
Penicillium
Pichia
Plectosphaerella
Podila
Polyporales_gen_Incertae_sedis
Pseudodactylaria
Pyronemataceae_gen_Incertae_sedis
Rozellomycota_gen_Incertae_sedis
Saccharomyces
Saitozyma
Scytalidium
Trichoderma
Unidentified_Ascomycota
Unidentified_Dipodascaceae
Unidentified_Dothideomycetes
Unidentified_Helotiales
Unidentified_Hypocreales
Unidentified_Mortierellaceae
Unidentified_Phaeosphaeriaceae
Unidentified_Saccharomycetales
Unidentified_Saccotheciaceae
Unidentified_Venturiales
Verticillium
Acinetobacter
Actinomyces
Alloprevotella
Aquamonas
Asaccharospora
Bacteroides
Bifidobacterium
Campylobacter
Capnocytophaga
Cellulosimicrobium
Clostridium sensu stricto 1
Conservatibacter
Corynebacterium
Enterobacter
Enterococcus
Fusobacterium
Gardnerella
Haemophilus
Klebsiella
Lachnoclostridium
Lachnospiraceae NK4A136 group
Leptotrichia
Neisseria
Other
Porphyromonas
Prevotella
Prevotella_7
Pseudomonas
Pseudoscardovia
Samsonia
Selenomonas
Staphylococcus
Streptococcus
Treponema
Unidentified_67-14
Unidentified_Bifidobacteriaceae
Unidentified_Cellulomonadaceae
Unidentified_Clostridiaceae
Unidentified_Enterobacteriaceae
Unidentified_Enterococcaceae
Unidentified_Geminicoccaceae
Unidentified_Lachnospiraceae
Unidentified_Lactobacillaceae
Unidentified_Methyloligellaceae
Unidentified_Muribaculaceae
Unidentified_Neisseriaceae
Unidentified_P5D1-392
Unidentified_Pasteurellaceae
Unidentified_Staphylococcaceae
Veillonella

Figure S2. Source contamination modeling. a) Fungal contaminate taxa detected by PERFect. b) Bacterial contaminate taxa detected by PERFect. c) Average abundance of filtered fungal taxa. d) Average abundance of filtered bacterial taxa. Please see tables of filtered taxa at github.com/WillisLungLab/MiBPD/SourceContamination.

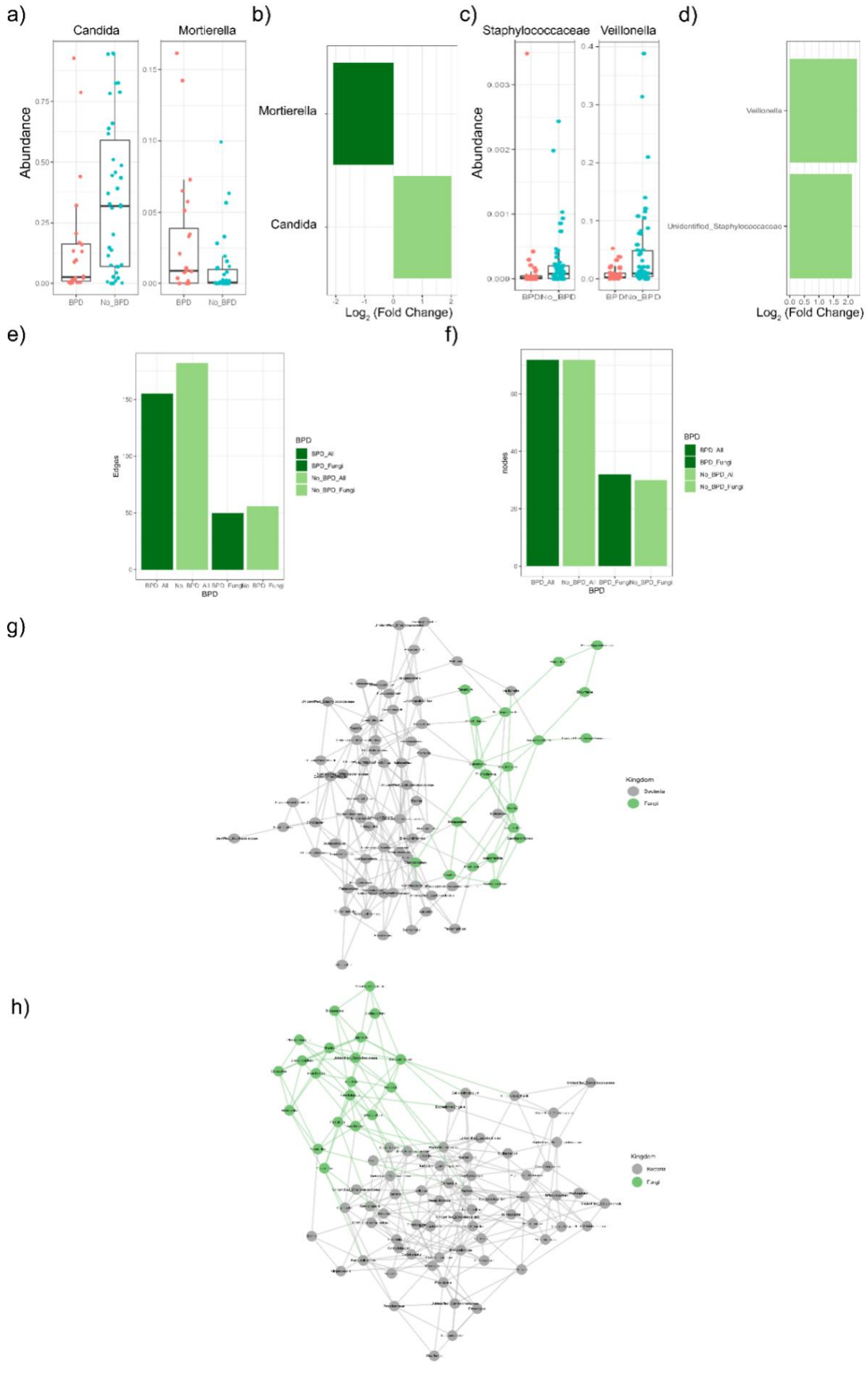
a)
Candida
Mortierella
Abundance
BPD
No_BPD
b)
Mortierella
Candida
Log2 (Fold Change)
c)
Staphylococcaceae
Veillonella
Abundance
d)
Veillonella
Unidentified_Staphylococcaceae
Log2 (Fold Change)
e)
Edges
BPD
BPD_All
BPD_Fungi
No_BPD_All
No_BPD_Fungi
f)
nodes
g)
Kingdom
Fungi
h)
Kingdom
Fungi

Figure S3. The BPD-associated mycobiome is unique. (a, b) Relative abundance of key fungi by DESeq2. (c,d) Relative abundance of key bacteria by DESeq2. (d) Number of edges in each SPIEC-EASI network. (e) Number of nodes in each SPIEC-EASI network. (e) Complete SPIEC-EASI BPD network with all genera labeled. (F) Complete NoBPD network with all genera labeled.

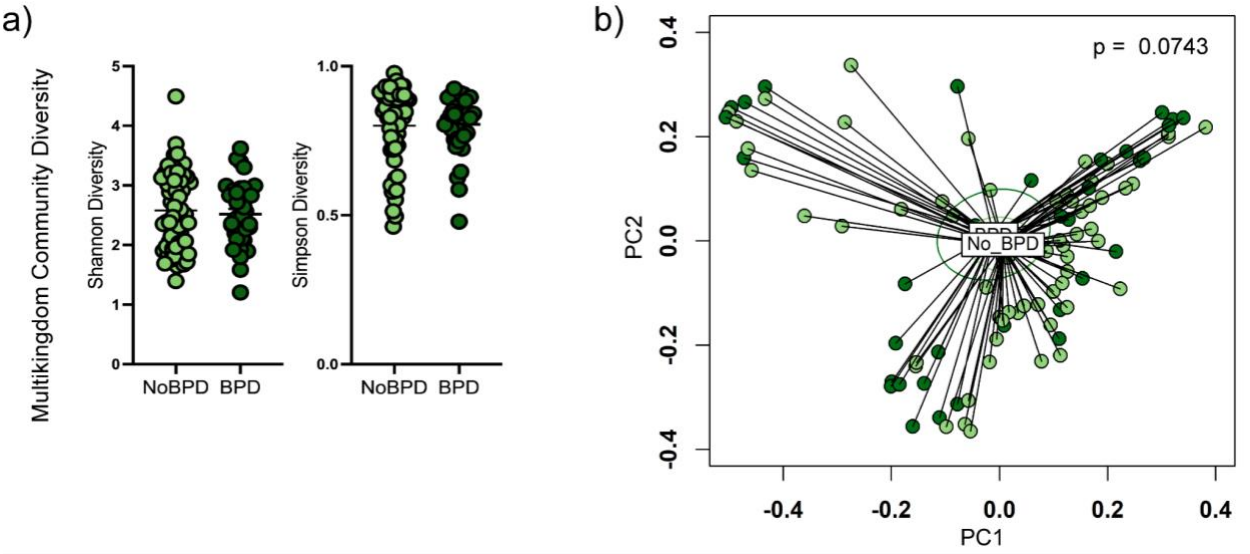

Figure S4. The overall composition of the multikingdom microbiome. (a) Alpha diversity. (c) Beta diversity (PCoA of Bray-Curtis dissimilarity, p = 0.0743, PERMANOVA, p = 0.3749, PERMDISP). Ellipses indicate the 95% confidence interval.

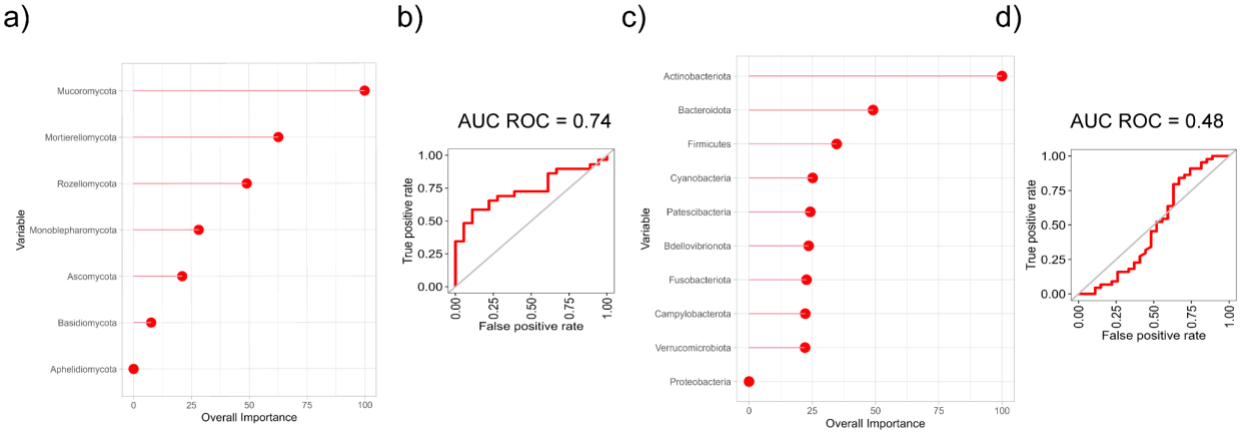

Figure S5. BPD status is predictable using machine-learning models of the fungal microbiota several weeks before the adjudication of the clinical diagnosis at 36 weeks corrected gestational age. (a-b) Exploratory random forest machine learning model

using genera level mycobiome and clinical data (Should be considered exploratory due to high risk of overfitting). (c-d) Exploratory random forest machine learning model using genera-level bacterial microbiota and clinical data.

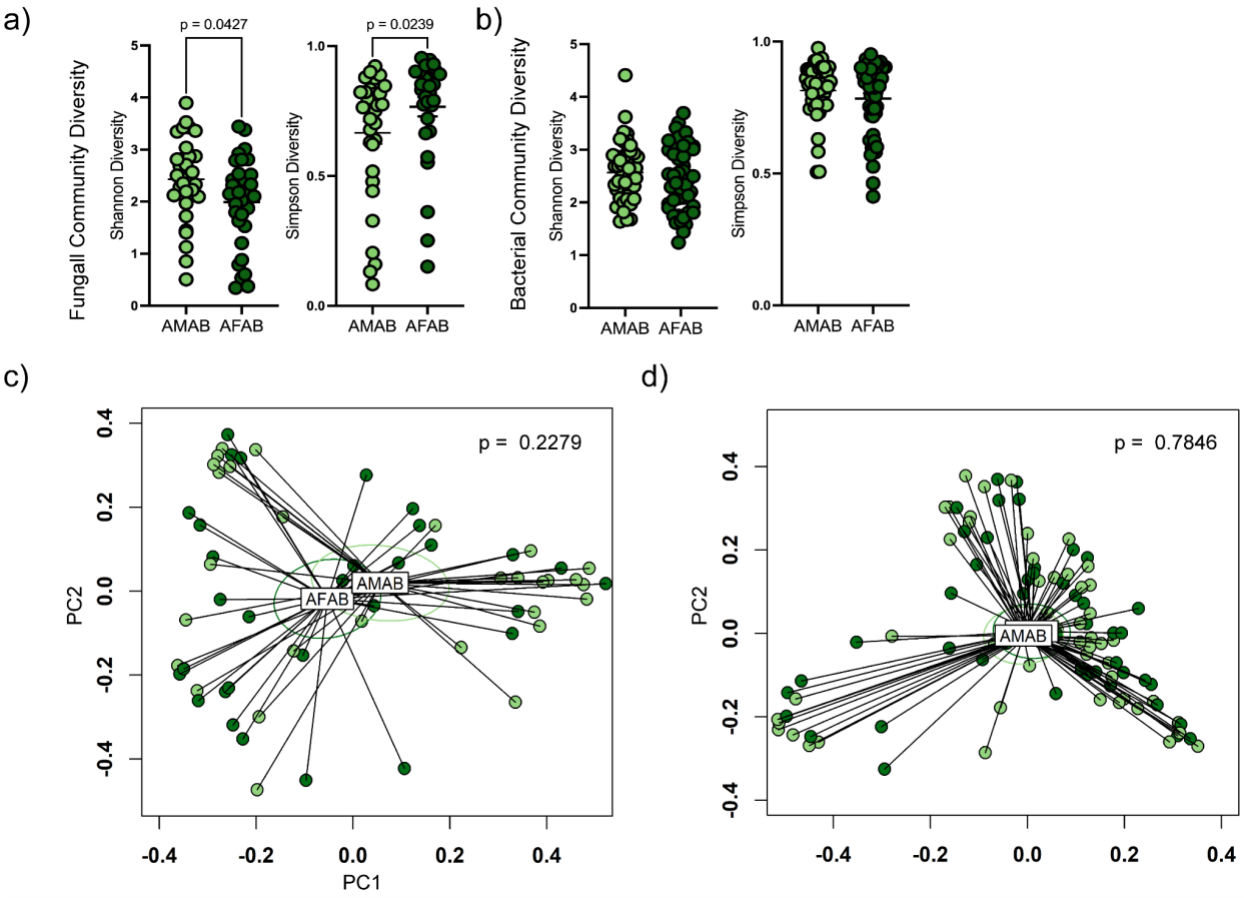

Figure S6. Mycobiome features differences by sex assigned at birth. (a) Fungal alpha diversity. (b) Bacterial alpha diversity. Shannon diversity decreased in infants assigned female at birth (AFAB) as compared to infants assigned male at birth (AMAB, p = 0.0427, Mann-Whitney). Simpson diversity was increased in infants AFAB as compared to those AMAB (p = 0.0239, Mann-Whitney). (c) Principal coordinates analysis of Bray-Curtis dissimilarity of fungal beta diversity (p = 0.2279, PERMANOVA; p = 0.9464, PERMDISP). (d) Principal coordinates analysis of Bray-Curtis dissimilarity of bacterial beta diversity (p = 0.7846, PERMANOVA; p = 0.3957, PERMDISP).

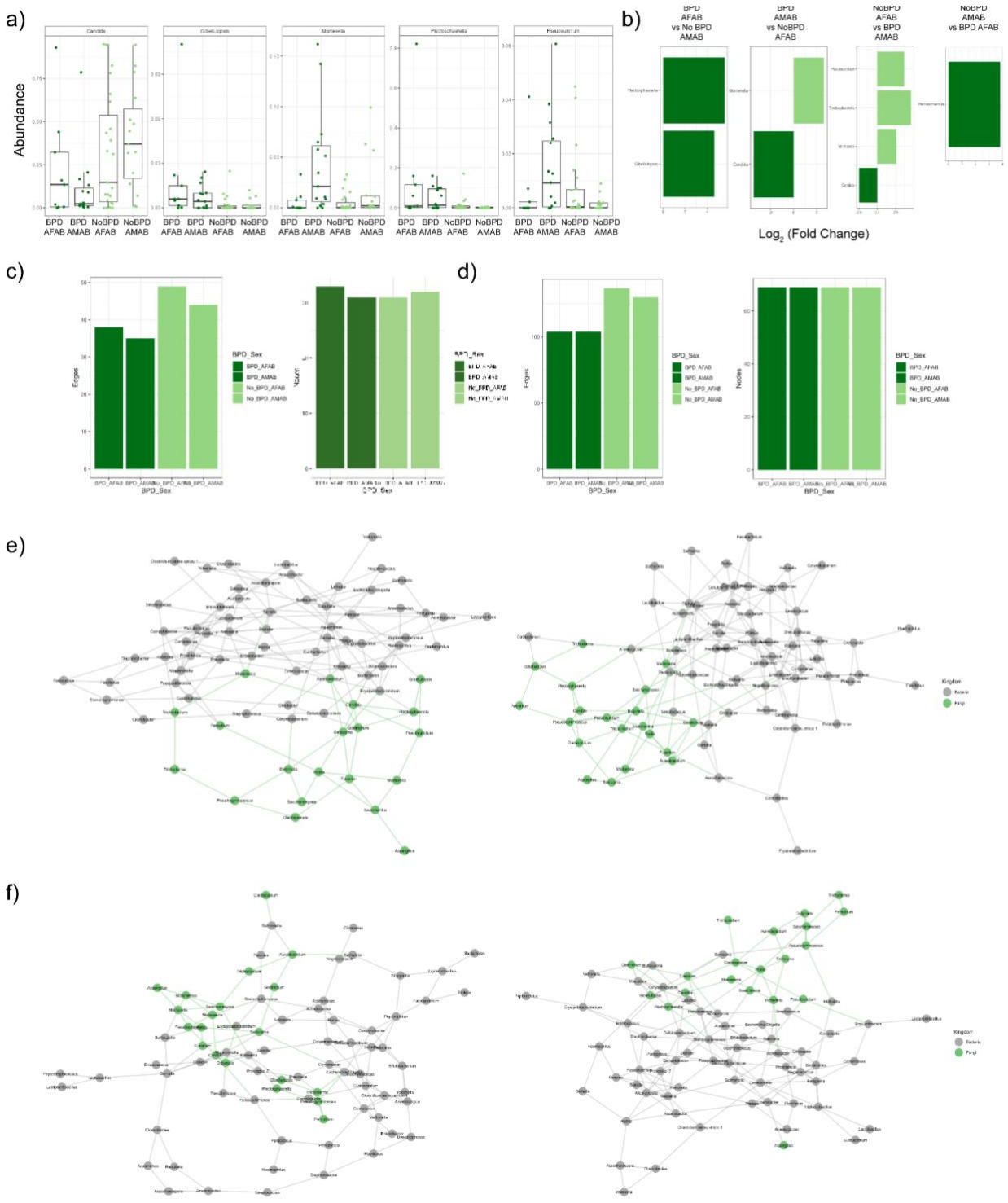

Figure S7. Microbiota alterations by disease status and sex assigned at birth. (a-b) DESeq2 selected features of the mycobiota. (c) SPIEC-EASI network edges. (d) SPIEC-EASI network nodes. (e) SPIEC-EASI networks for NoBPD infants assigned male at birth (AMAB) or assigned female at birth (AFAB). (f) SPIEC-EASI networks for BPD infants.

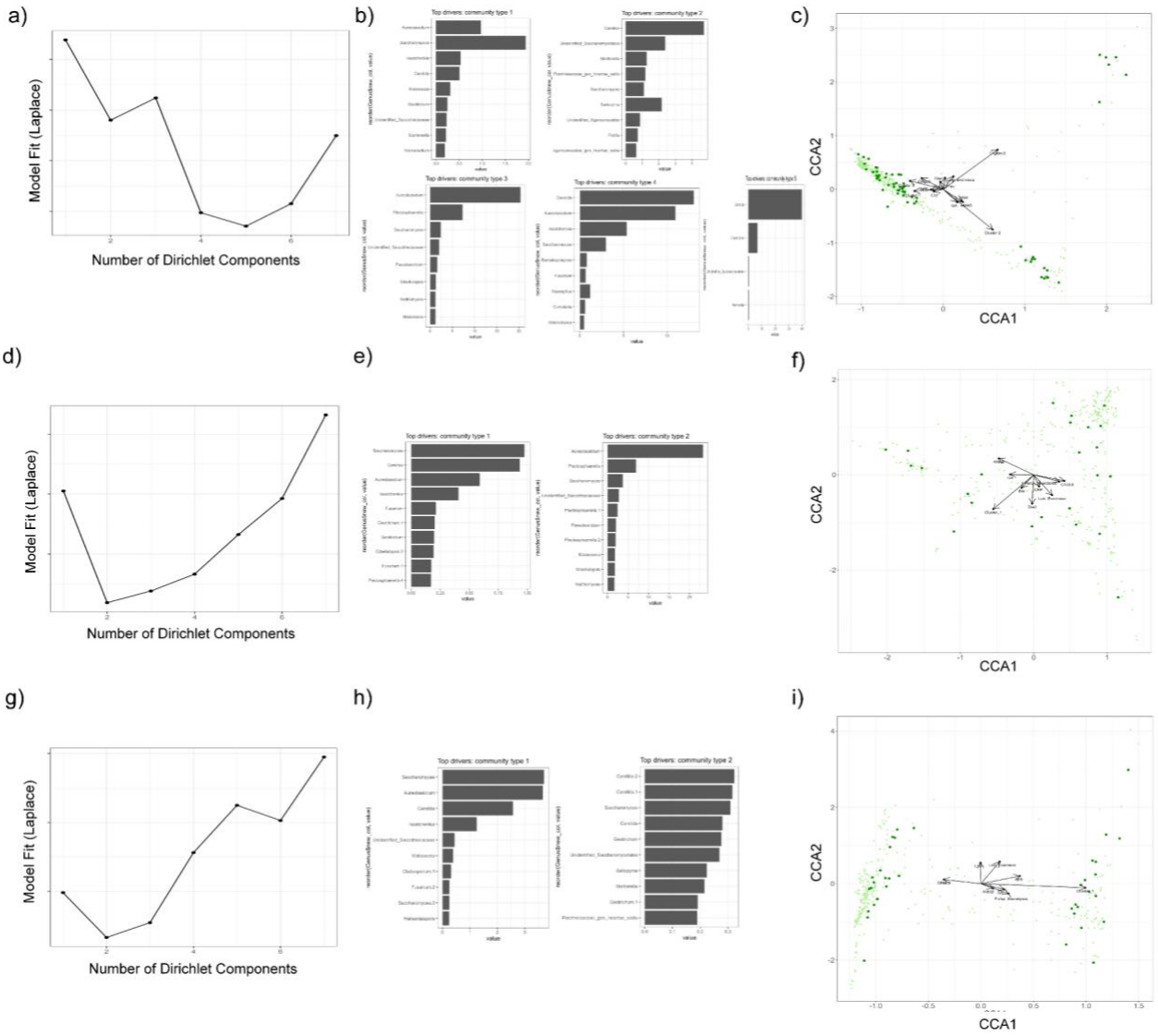

Figure S8. Dirichlet-Multinomial Mixture (DMM) modeling of the mycobiome. (a) Laplace analysis of the mycobiome indicates optimal model fit points with 5 clusters. (b) Variable importance analysis of the fungal DMM model. (c) Canonical Correspondence Analysis (CCA) for the DMM model. (d) Laplace analysis of mycobiome samples from NoBPD infants shows an optimal fit point at 2 clusters. (e) Variable importance analysis of the NoBPD DMM model. (f) CCA for the NoBPD DMM model. (g) Laplace analysis of mycobiome samples from BPD infants shows an optimal fit point at 2 clusters. (h) Variable importance analysis of the BPD DMM model. (i) CCA for the BPD DMM model.

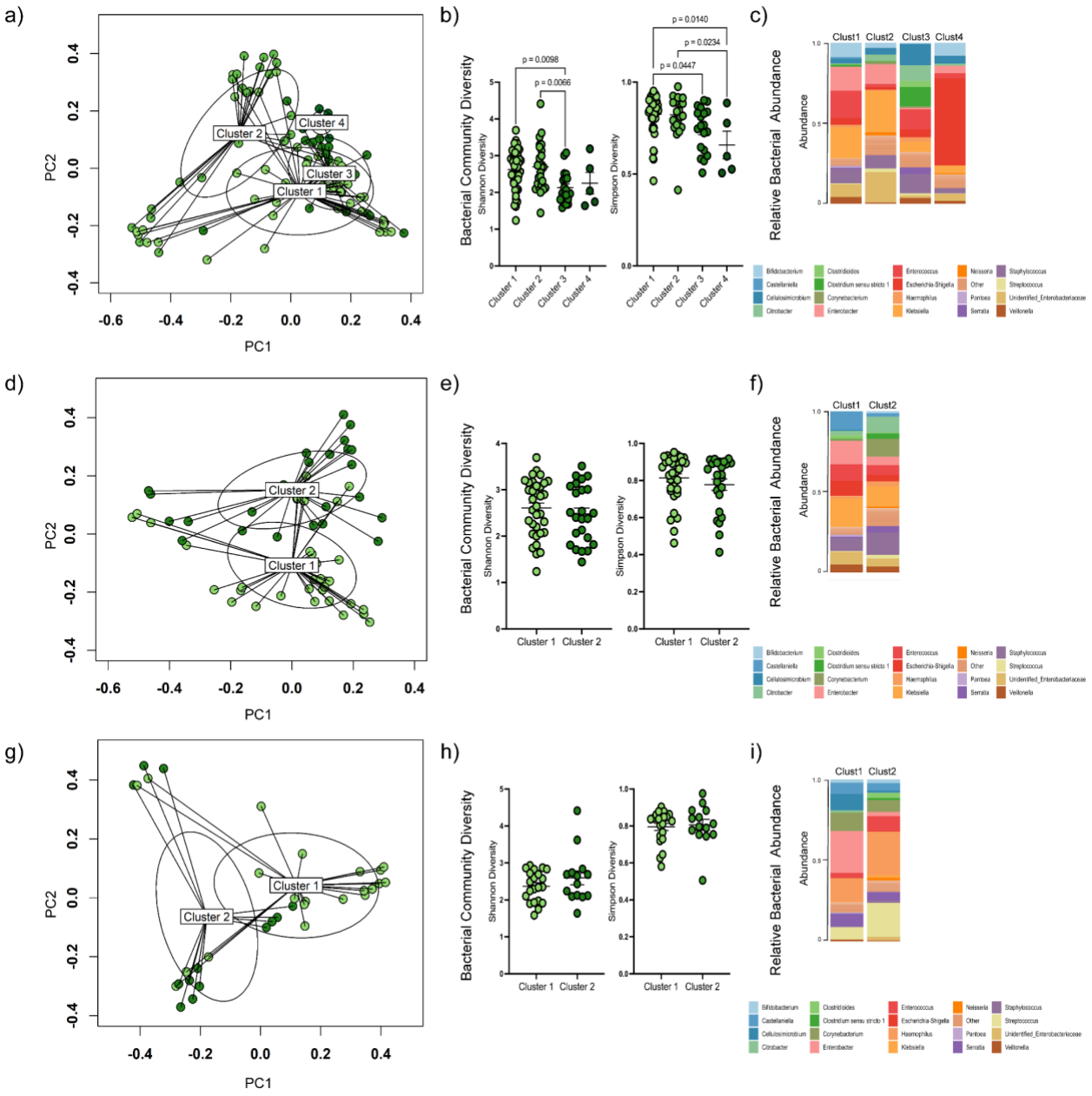

Figure S9. Dirichlet-Multinomial Mixture (DMM) modeling of the bacterial microbiome. (a) Principal Coordinates Analysis (PCoA) of the bacterial microbiome DMM model. (b) Alpha diversity of the bacterial microbiome DMM model. (c) Relative abundance of the bacterial microbiome in the DMM components. (d) PCoA of the DMM model of the bacterial microbiome of infants with NoBPD. (e) Alpha diversity of the multikingdom microbiome. (f) Relative abundance of the bacterial microbiome in the NoBPD DMM model. (g) PCoA of the DMM model of the bacterial microbiome of infants with BPD. (h) Alpha diversity of the bacterial microbiome. (i) Relative abundance of the multikingdom microbiome in the BPD DMM model. Ellipses indicated the 95% confidence interval.

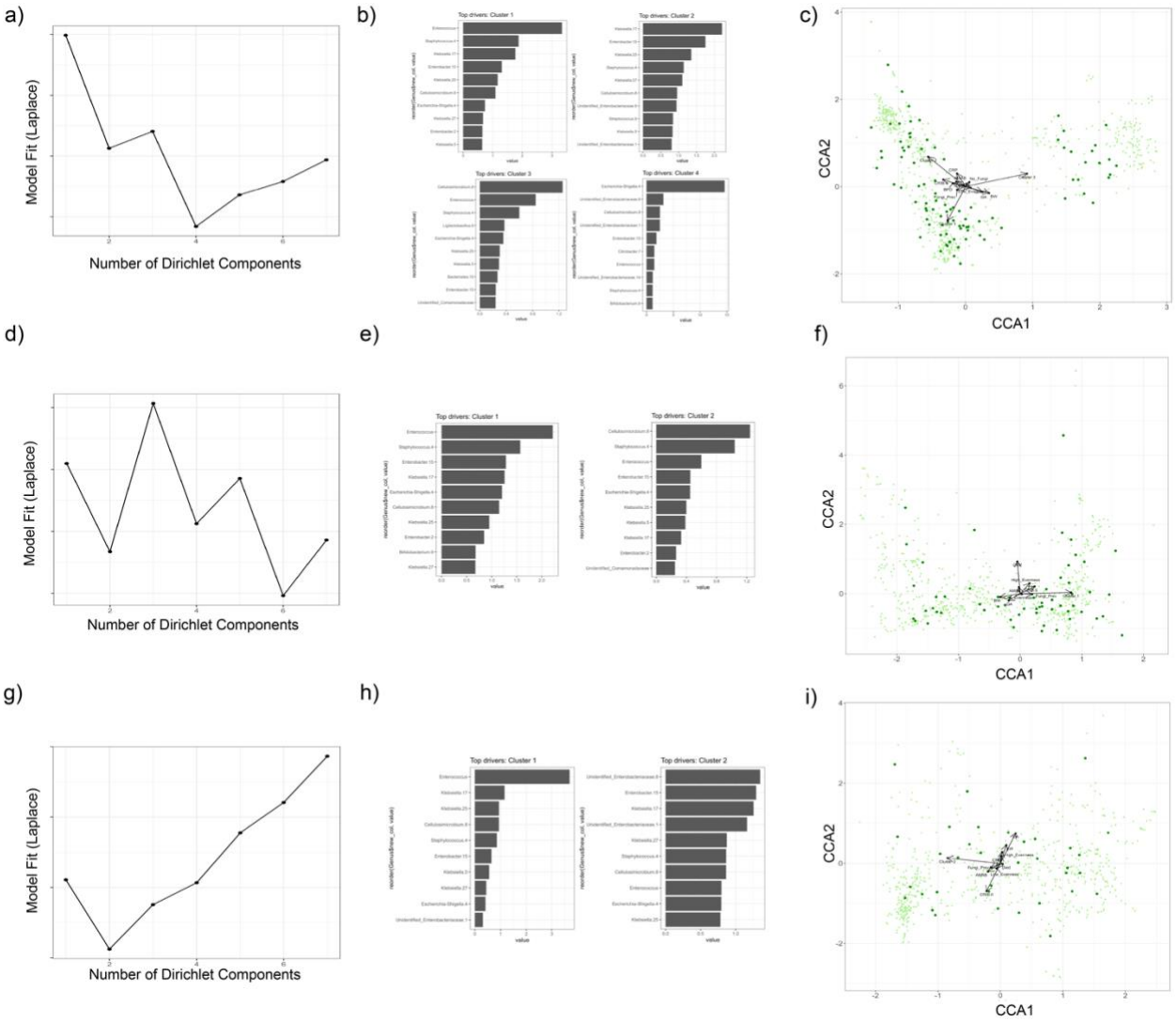

Figure S10. DMM modeling of the bacterial microbiome. (a) Laplace analysis of the mycobiome indicates an optimal model fit point with four components. (b) Variable importance analysis of the multikingdom microbiome DMM model. (c) Canonical Correspondence Analysis (CCA) for the multikingdom microbiome DMM model. (d) Laplace analysis of multikingdom microbiome samples from NoBPD infants shows an optimal fit point at three components. (e) Variable importance analysis of the NoBPD DMM model. (f) CCA for the NoBPD DMM model. (g) Laplace analysis of multikingdom microbiome samples from BPD infants shows an optimal fit point at two components. (h) Variable importance analysis of the BPD DMM model. (i) CCA for the BPD DMM model.

Figure S11. Comparison between the fungal microbiomes of FMT-colonized and SPF control mice.

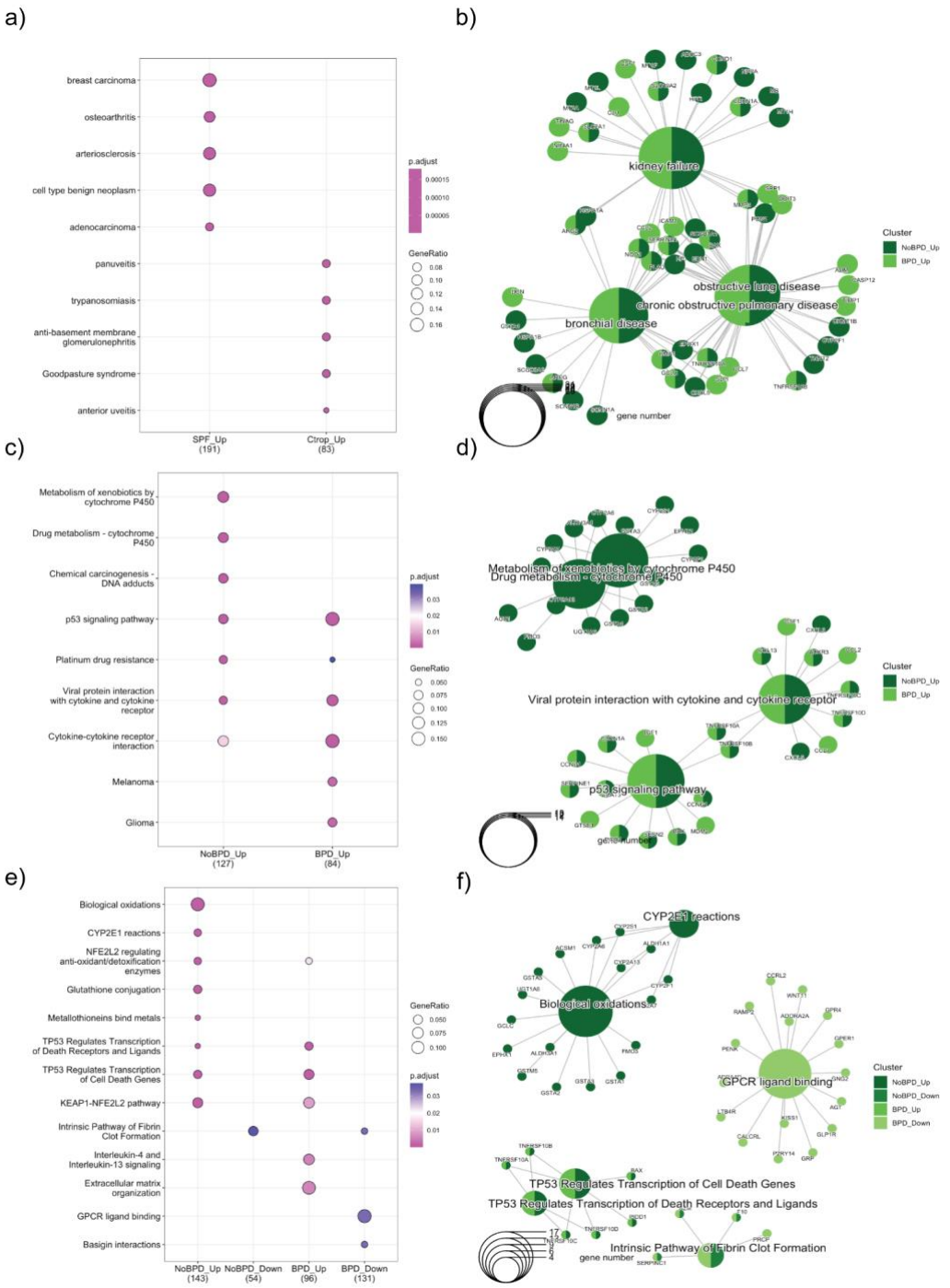

Figure S12. Comparative RNA-seq pathway analysis for fecal microbiota transfer experiment. Comparative gene enrichment analysis was performed using the top UP and DOWN regulated genes in NoBPD hyperoxia vs NoBPD normoxia compared to BPD hyperoxia vs NoBPD normoxia top regulated genes. Top pathways (based on adjusted p-value) are shown. (a) Top (5) Disease Ontology terms between BPD-FMT HO and NoBPD-FMT NO mice. (b) Network of top (2) DO terms and genes. (c) Top (5)

KEGG pathways between BPD-FMT HO and NoBPD-FMT NO mice. (d) Network of top (2) KEGG pathways and genes. (c) Top (5) Reactome pathways between BPD-FMT HO and NoBPD-FMT NO mice. (d) Network of top (2) Reactome pathways and genes.

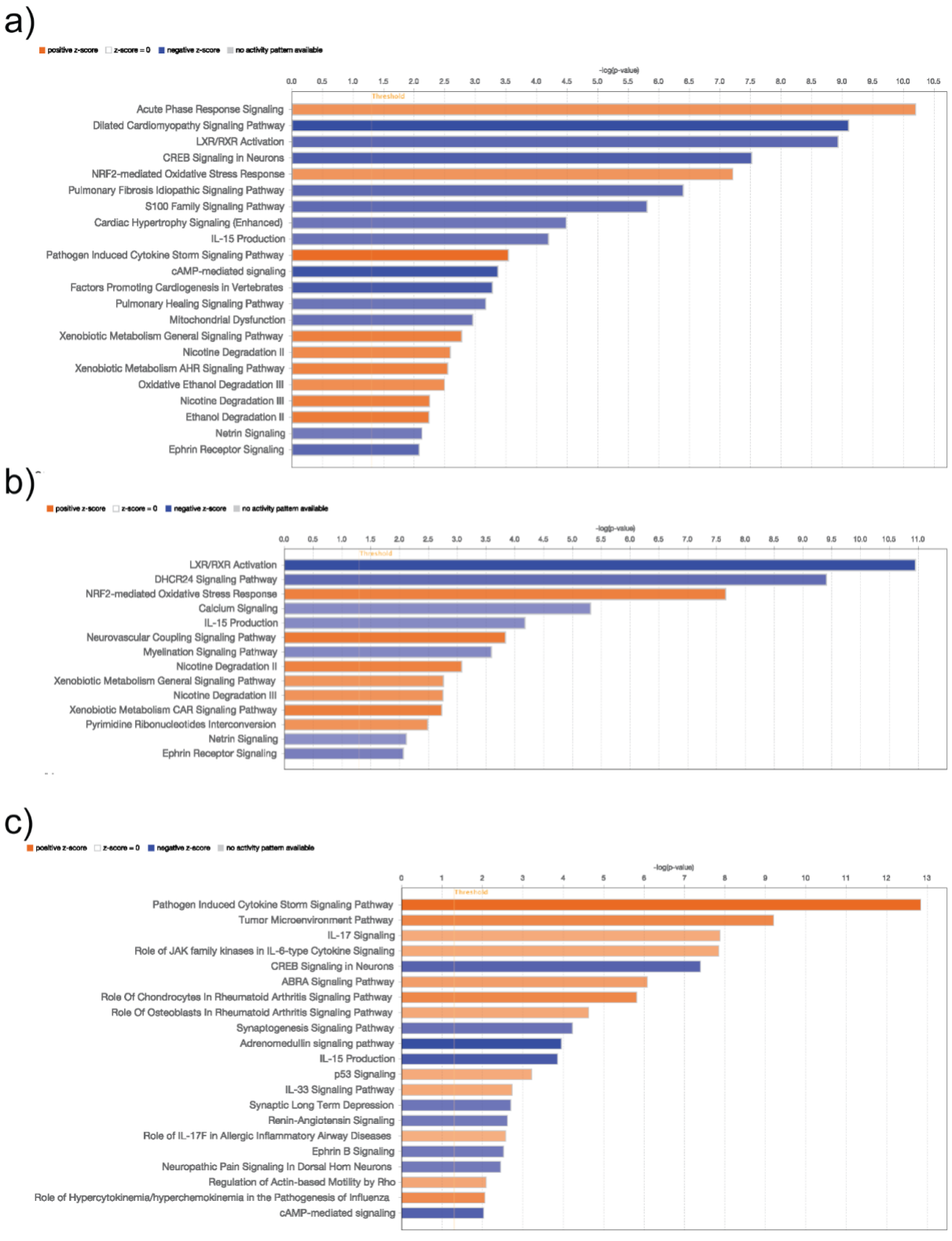

Figure S13. Ingenuity pathway analysis. (A) Pathways in BPD-FMT mice. (B) Pathways in NoBPD-FMT mice. (C) Pathways in specific pathogen-free (SPF) mice.

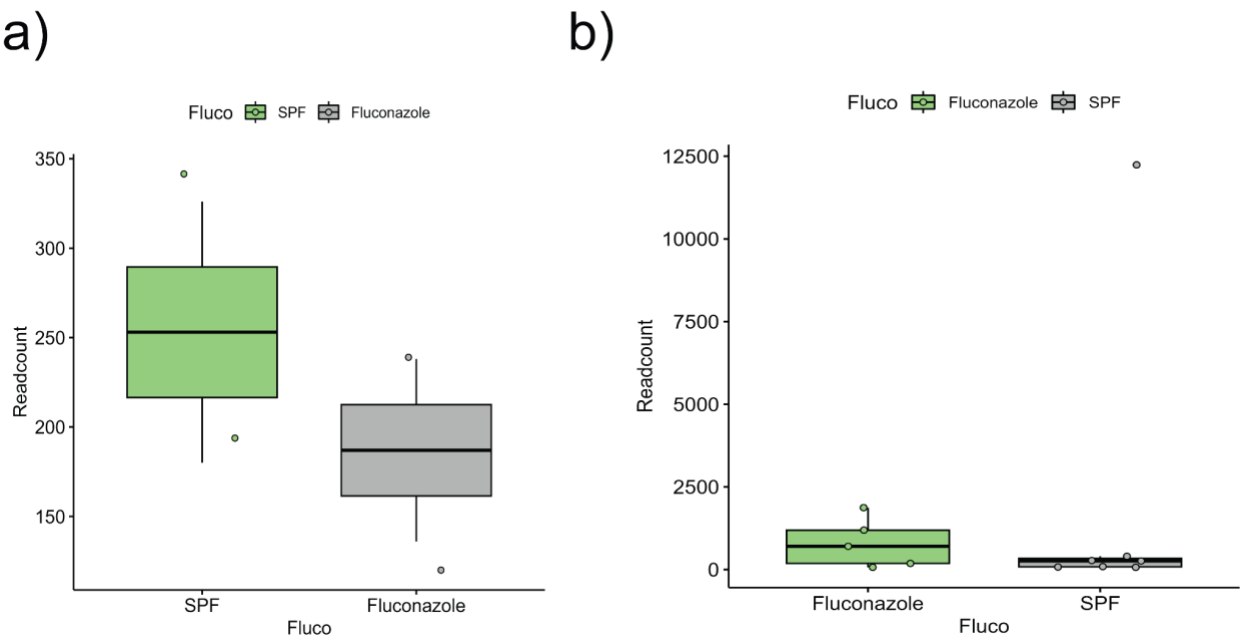

Figure S14. Read counts in fluconazole-exposed neonatal mice. (a) ITS2 read counts in neonatal mouse gut samples. (b) ITS2 read counts in neonatal mouse lung samples.

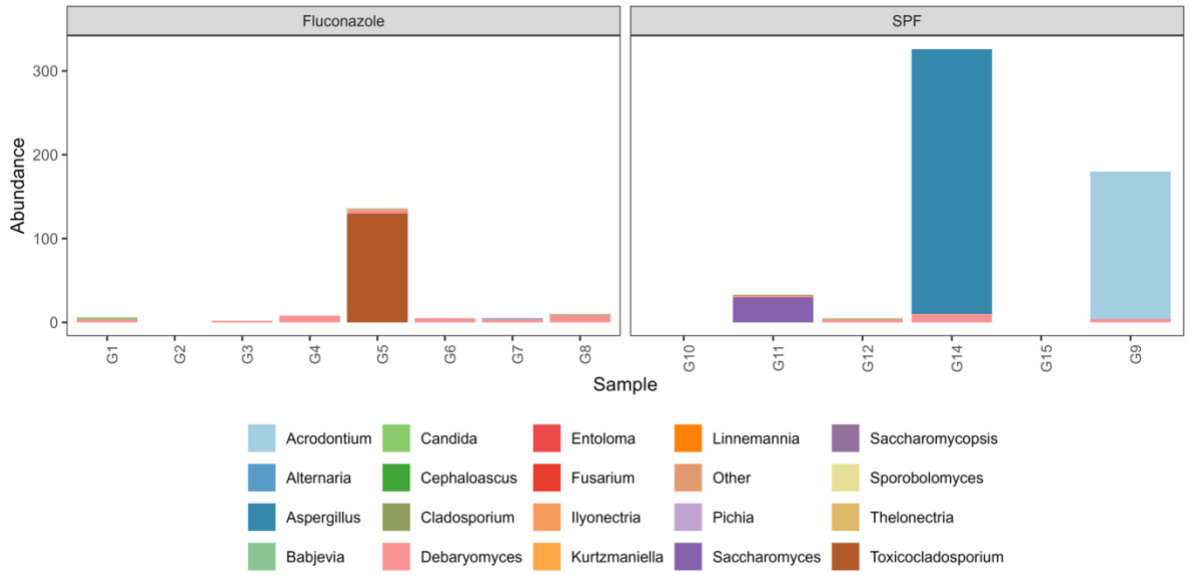

Figure S15. Relative abundance of fungal genera between fluconazole and control mice. Potential antifungal amplification of selected fungal colonization occurred in only one sample (G5). Of note, absolute fungal colonization in the fluconazole-exposed group is so low, no significant differences could be detected by DESeq2.

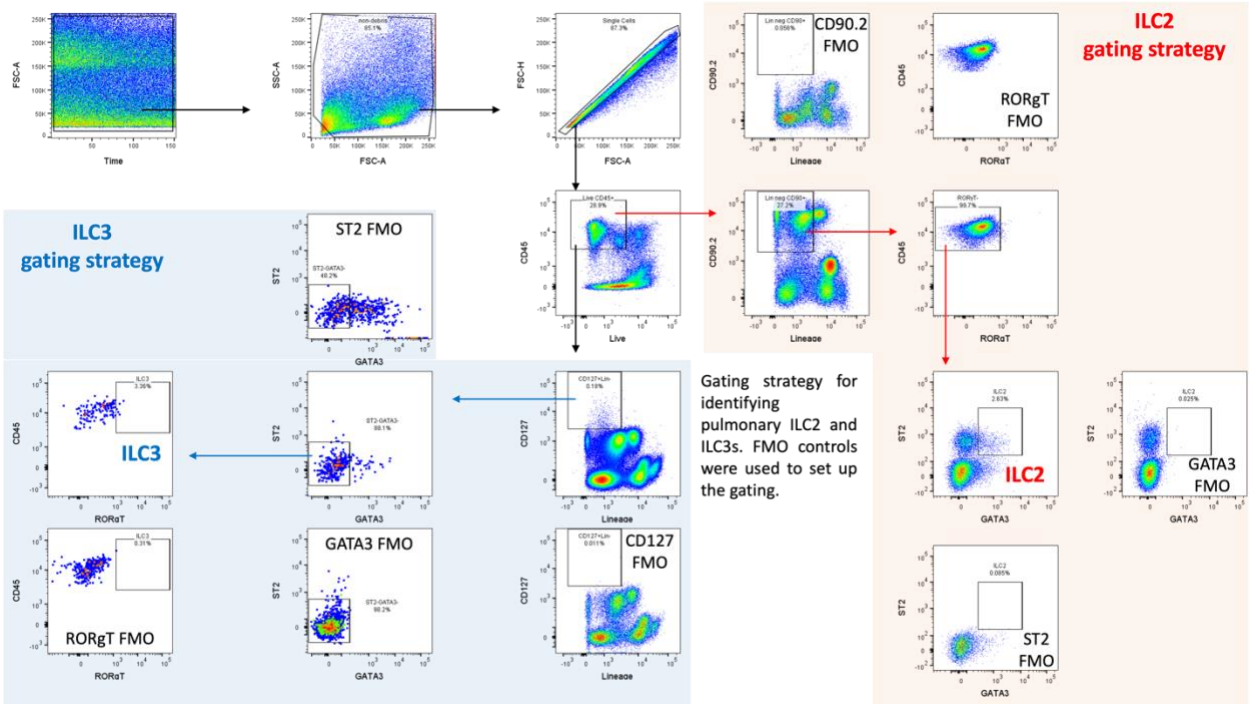

Figure S16. Flow cytometry gating strategy. ILC2s were defined as live, lineage negative, ST2+CD127+Gata3+ cells. FMO, fluorescence minus one.

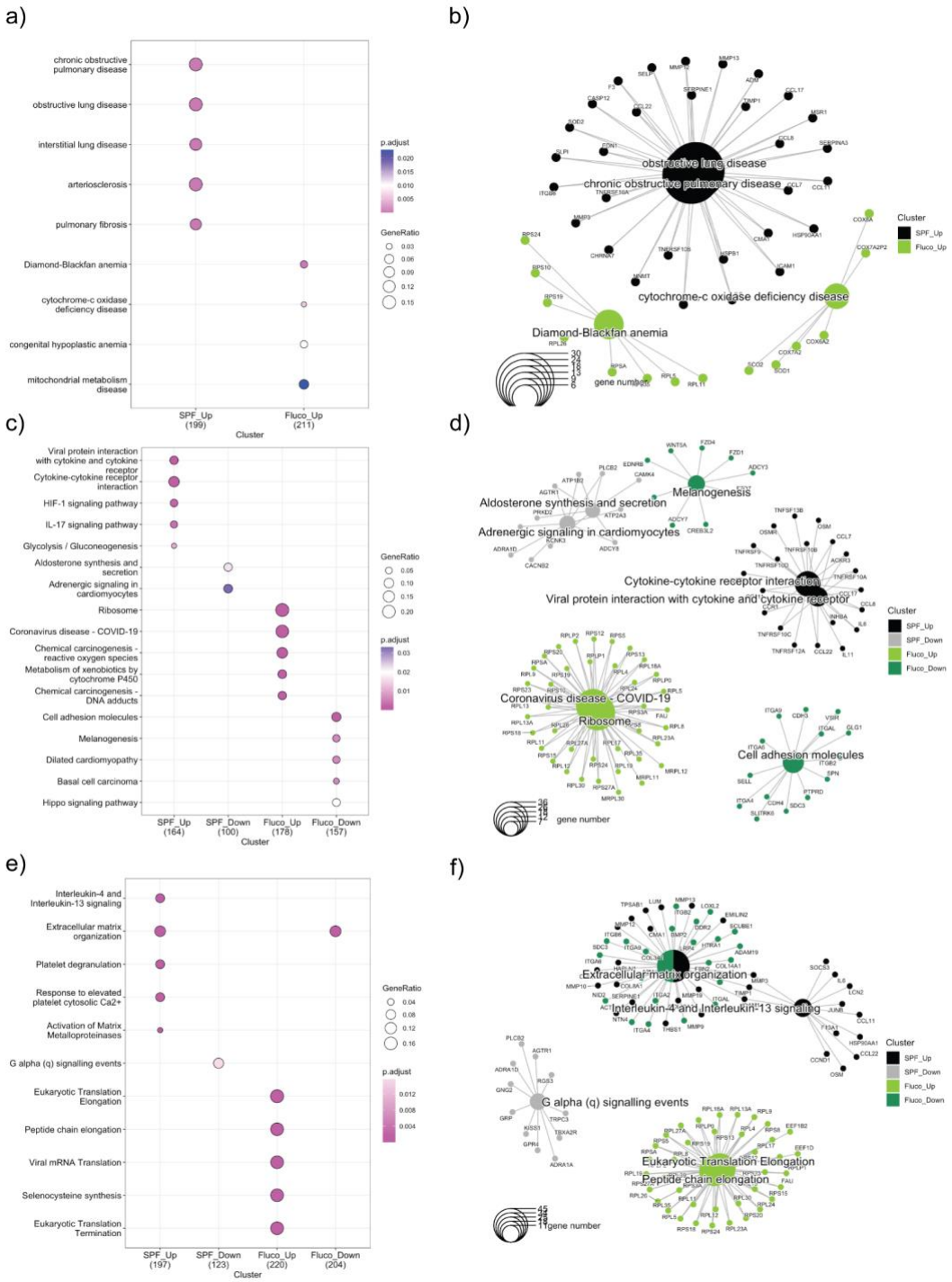

Figure S17. RNA-seq pathway analysis of fluconazole-exposed mice. (a) Significant Disease Ontology terms between Fluco HO and SPF NO mice. (b) Network of significant DO terms and genes. (c) Significant KEGG pathways between Fluco HO and SPF NO mice. (d) Network of significant KEGG pathways and genes. (c) Significant Reactome pathways between Fluco HO and SPF NO mice. (d) Network of significant Reactome pathways and genes.

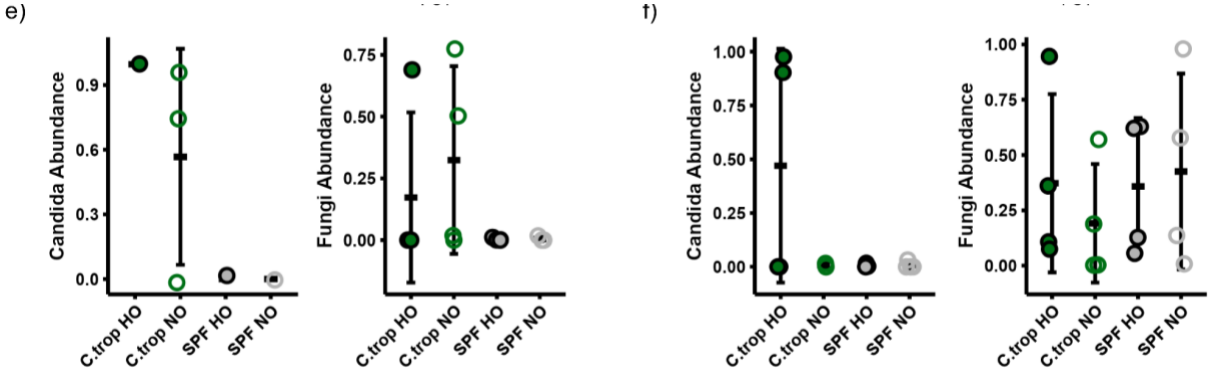

Figure S18. (e) Gut *Candida* and total fungal relative abundance. (f) Lung *Candida* and total fungal relative abundance.

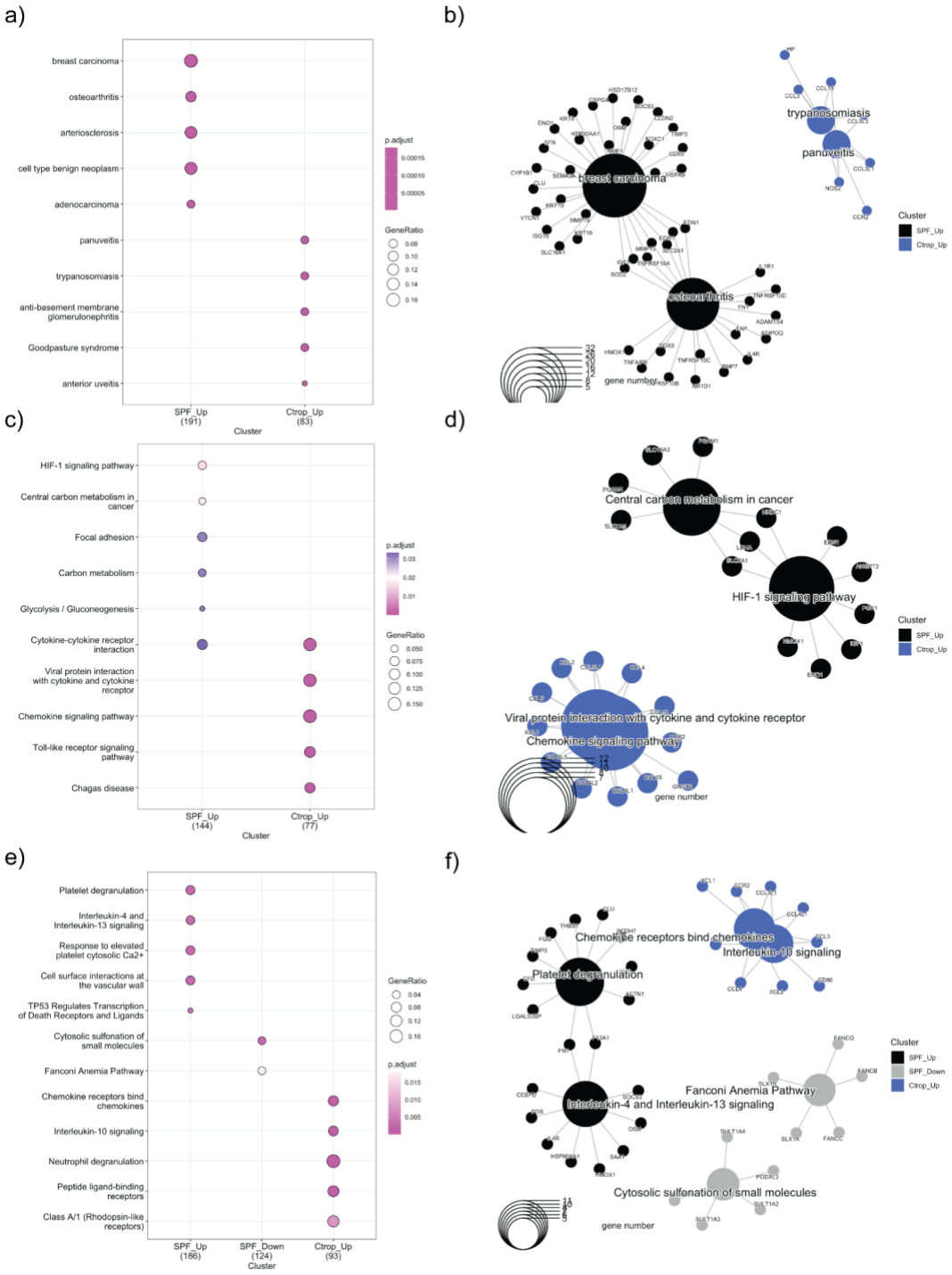

Figure S19. RNA-seq pathway analysis of *C.tropicalis*-colonized mice. (a) Significant Disease Ontology terms between *C.trop* HO and SPF NO mice. (b) Network of significant DO terms and genes. (c) Significant KEGG pathways between *C.trop* HO and SPF NO mice. (d) Network of significant KEGG pathways and genes. (c) Significant Reactome pathways between *C.trop* HO and SPF NO mice. (d) Network of significant Reactome pathways and genes.

Tables:

Table S1. Cohort characteristics and demographics

	NoBPD	**BPD**	**n**	***p***
Median (IQR) or n (%)	64	38		
Gestational age (weeks)	29.0 (27.6 - 30.8)	25.7 (25 - 27.8)	102	< 0.001
Birthweight (g)	1145 (840 - 1330)	775 (670 - 860)	102	< 0.001
Female sex assigned at birth	37/64 (57.8%)	14/38 (36.8%)	102	0.041
Antenatal Steroids (No)	8/47 (17%)	4/30 (13.3%)	77	0.33
Surfactant (None)	27/62 (43.5%)	1/38 (2.6%)	100	<0.001
Apgar score (1 min)	6 (3 - 7)	4 (2 - 5)	99	< 0.001
Apgar score (5 min)	7 (6 - 8)	6 (5 - 7)	99	< 0.001
Small for gestational age*	6/64 (9.4%)	8/38 (21.1%)	102	0.098
Cesarean section (1)	28/47 (59.6%)	20/30 (66.7%)	77	0.531
Prolonged rupture of membranes** (1)	7/47 (15%)	5/30 (16.7%)	77	0.834
Critical Risk Index for Babies II (CRIB II) score	7 (4 - 9)	12 (9 - 14)	95	< 0.001
Prenatal antibiotic exposure	22/47 (46.8%)	15/30 (50%)	77	0.785
Duration of prenatal antibiotic exposure (d)	1 (0 - 1)	0 (0 - 1)	60	0.542
Postnatal antibiotic exposure	55/64 (85.9%)	38/38 (100%)	102	0.015
Duration of postnatal antibiotic exposure (d)	2 (1 - 2)	2 (1 - 4)	96	0.016
Endotracheal intubation	41/62 (66.1%)	37/37 (100%)	99	< 0.001

Ventilation duration (d)	1 (0 - 4)	34 (22 - 50)	94	< 0.001
Non-invasive ventilation duration (d)	5 (1 - 17)	14 (1 - 38)	94	0.053
Oxygen exposure duration (d)	13 (4 - 41)	92 (30 - 119)	94	< 0.001
Death	1/63 (1.6%)	6/38 (15.8%)	101	0.006

Data are presented as median (interquartile range) or n (%) with significance testing by Mann-Whitney U or Pearson chi-squared test, as appropriate.

BPD, Bronchopulmonary dysplasia; NoBPD, Post-prematurity respiratory disease. *< 3rd percentile, ‡ > 18 h, †NICHD Neonatal Outcomes Estimator

Table S2. Characteristics and demographics of infants without a stool for analysis

	Not Sequenced n = 42	Sequenced n = 102	Total N	*P*
Median (IQR) or n (%)				
Gestational age (weeks)	28.0 (26.1 - 29.8)	28.0 (25.8 - 30)	144	0.778
Birthweight (g)	950 (740 - 1160)	905 (760 - 1290)	144	0.733
Female sex assigned at birth	20/42 (47.6%)	51/51 (50%)	144	0.795
Antenatal Steroids (No)	10/35 (28.6%)	12/77 (15.6%)	112	0.421
Surfactant (None)	12/39 (30.8%)	28/100 (28.0)%	139	0.078
Apgar score (1 min)	4 (1 - 6)	5 (3 - 7)	133	0.26
Apgar score (5 min)	7 (5 - 8)	7 (5 - 8)	134	0.491
Small for gestational age*	4/42 (9.5%)	14/102 (13.7%)	144	0.488
Cesarean section (1)	25/35 (71.4%)	48/77 (62.3%)	112	0.349
Prolonged rupture of membranes** (1)	7/35 (20.0%)	12/77 (15.6%)	112	0.564
Critical Risk Index for Babies II (CRIB II) score	9 (7 - 12)	9 (6 - 12)	134	0.499
Prenatal antibiotic exposure	22 (46.8%)	15 (50%)	112	0.323
Postnatal antibiotic exposure	37/42 (88.1%)	93/102 (91.2%)	144	0.571
Duration of postnatal antibiotic exposure (d)	2 (1 - 2)	2 (1 - 2)	133	0.635
Endotracheal intubation	30/41 (73.2%)	78/99 (78.8%)	140	0.471
Ventilation duration (d)	4 (0 - 16)	3 (0 - 26)	135	0.635
Non-invasive ventilation duration (d)	4 (1 - 15)	7 (1 - 19)	135	0.201

Oxygen exposure duration (d)	25 (8 - 68)	31 (8 - 76)	135	0.464
Death	4/41 (9.8%)	11/142 (7.7%)	142	0.568
BPD rates	19/41 (46.3%)	38/102 (37.3%)	143	0.316

Table S3. PERMANOVA analysis of potential fungal covariates.

ITS Covariates	Sum of Squares	R^2	F	*p*	*q* (FDR)
Oxygen (days)	0.859912	0.040065	2.420743	0.010199	0.078192
Death	0.251176	0.01127	0.683911	0.785721	0.90358
Sex	0.454867	0.02041	1.250084	0.227877	0.403167
Gestational Age	0.502412	0.022543	1.383761	0.161084	0.308744
Birthweight	0.668982	0.030017	1.856733	0.045995	0.176316
CRIB-II	0.675101	0.030291	1.874244	0.044296	0.176316
Intubation	0.626614	0.028479	1.729528	0.062794	0.180762
Vent (days)	0.928147	0.043244	2.621516	0.005599	0.074743
Maternal UTI	0.291891	0.019745	0.90643	0.513049	0.737507
Preeclampsia	0.848091	0.05737	2.738757	0.006499	0.074743
Cesarean Section	0.568242	0.038439	1.798908	0.065493	0.180762
Multiples	0.128391	0.008685	0.394254	0.968403	0.968403
IUGR	0.361984	0.024487	1.129558	0.318868	0.523855
Feeding	1.249595	0.056793	0.842982	0.785421	0.90358
Prenatal Abx	0.220037	0.016129	0.704909	0.70443	0.90358
Postnatal Abx	0.60025	0.028093	1.676481	0.071393	0.180762
NEC	0.26655	0.012115	0.723522	0.765623	0.90358
Culture+ Sepsis	0.365213	0.016599	0.995854	0.410059	0.628757
Culture- Sepsis	0.507824	0.02308	1.393907	0.151385	0.308744

CRP	0.221336	0.009931	0.601845	0.857114	0.938744

Table S4. PERMANOVA analysis of potential bacterial covariates.

Bacterial Covariates	**Df**	**Sum of Sqs**	**R^2**	**F**	***p***	***q* (FDR)**
Death	1	0.174478	0.005424	0.496284	0.986401	0.986401
Sex	1	0.259828	0.008077	0.74103	0.784622	0.859347
Gestational age	1	0.583988	0.018155	1.682631	0.037496	0.172483
Birthweight	1	0.738424	0.022956	2.138061	0.005999	0.10349
CRIB-II	1	0.630824	0.019611	1.820278	0.022698	0.130512
Feeding	4	1.383682	0.044219	0.994685	0.480952	0.655051
Oxygen (days)	1	0.526242	0.017615	1.524152	0.072893	0.20468
Vent (days	1	0.368035	0.01232	1.060221	0.373363	0.572489
Multiples	1	0.31171	0.013528	0.946218	0.484952	0.655051
IUGR	1	0.362514	0.015733	1.102904	0.322868	0.530426
Maternal UTI	1	0.297311	0.012903	0.901938	0.554045	0.663484
Preeclampsia	1	0.439966	0.019094	1.343129	0.161984	0.312769
Cesarean section	1	0.21574	0.009363	0.652141	0.838816	0.876944
Prenatal Abx	1	0.557406	0.026794	1.734477	0.008999	0.10349
Postnatal Abx	1	0.451244	0.014831	1.29471	0.163184	0.312769

NEC	1	0.309181	0.009881	0.888147	0.576942	0.663484
Intubation	1	0.537091	0.017164	1.55427	0.069293	0.20468
Culture+ sepsis	1	0.474332	0.015158	1.369859	0.123588	0.284252
Culture- sepsis	1	0.668253	0.021356	1.942117	0.015398	0.118055
CRP	1	0.329732	0.01037	0.943039	0.512649	0.655051

Table S5. Type 2 Innate Lymphoid Cell Flow Cytometry Panel

Antibody	**Conjugate**	**Dilution**	**Company - Cat #**	**RRID**
CD90.2 (Thy1.2)	FITC	1:100	Biolegend - 105306	RRID:AB_313177
CD127 (IL-7Rα)	APC	2:100	Biolegend - 135012	RRID:AB_1937216
CD45	APC/Cyanine7	1:100	Biolegend - 103116	RRID:AB_312981
IL-33R (ST2)	PE	5:100	TFS - 12-9333-82	RRID:AB_2572706
RORγt	PerCP-Cy™5.5	5:100	BD Biosciences - 562683	RRID:AB_2737720
GATA3	PE-Cy™7	5:100	BD Biosciences - 560405	RRID:AB_1645544
Lineage Mix				
CD3ε (17A2)	violetFluor™ 450	1:100	TonboBio - 75-0032	RRID:AB_2621923
CD3ε	BUV 737	2:100	BD - 612771	RRID:AB_2870100

CD19	Pacific Blue™	2:100	Biolegend - 115526	RRID:AB_493341
CD11b	Pacific Blue™	2:100	Biolegend - 101224	RRID:AB_755986
CD11c	Pacific Blue™	2:100	Biolegend - 117321	RRID:AB_755987
CD49b	Pacific Blue™	2:100	Biolegend - 108918	RRID:AB_2265144
F4/80	Pacific Blue™	1:100	Biolegend - 123123	RRID:AB_893487
FcεRIα	Pacific Blue™	1:100	Biolegend - 134313	RRID:AB_10612933
Ly6G	Pacific Blue™	1:100	Biolegend - 127611	RRID:AB_1877212
Live/Dead, UV	350 - 450	1:1000	Invitrogen - L23105	

References:

1. Willis, K.A., Purvis, J.H., Myers, E.D., Aziz, M.M., Karabayir, I., Gomes, C.K., Peters, B.M., Akbilgic, O., Talati, A.J., and Pierre, J.F. (*2019*). Fungi form interkingdom microbial communities in the primordial human gut that develop with gestational age. FASEB journal : official publication of the Federation of American Societies for Experimental Biology *33*, 1*2825*–12*837*. https://doi.org/*10*.1096/fj.201901*4*36rr.
2. Higgins, R.D., Jobe, A.H., Koso-Thomas, M., Bancalari, E., Viscardi, R.M., Hartert, T.V., Ryan, R.M., Kallapur, S.G., Steinhorn, R.H., Konduri, G.G., et al. (2018). Bronchopulmonary Dysplasia: Executive Summary of a Workshop. J Pediatrics *197*, 300–308. https://doi.org/10.1016/j.jpeds.2018.01.043.
3. Laughon, M.M., Langer, J.C., Bose, C.L., Smith, P.B., Ambalavanan, N., Kennedy, K.A., Stoll, B.J., Buchter, S., Laptook, A.R., Ehrenkranz, R.A., et al. (2011). Prediction of Bronchopulmonary Dysplasia by Postnatal Age in Extremely Premature Infants. Am J Resp Crit Care *183*, 1715–1722. https://doi.org/10.1164/rccm.201101-0055oc.
4. Elm, E. von, Altman, D.G., Egger, M., Pocock, S.J., Gøtzsche, P.C., Vandenbroucke, J.P., and Initiative, S. (2007). The Strengthening the Reporting of Observational Studies

in Epidemiology (STROBE) Statement: Guidelines for Reporting Observational Studies. Plos Med 4, e*296*. https://doi.org/10.*13*71/journal.pmed.0040296.
5. Kilkenny, C., Browne, W.J., Cuthill, I.C., Emerson, M., and Altman, D.G. (2010). Improving bioscience research reporting: the ARRIVE guidelines for reporting animal research. Preprint.
6. Staley, C., Kaiser, T., Beura, L.K., Hamilton, M.J., Weingarden, A.R., Bobr, A., Kang, J., Masopust, D., Sadowsky, M.J., and Khoruts, A. (2017). Stable engraftment of human microbiota into mice with a single oral gavage following antibiotic conditioning. Microbiome 5, 87. https://doi.org/10.1186/s40168-017-0306-2.
7. Chen, X., Li, P., Liu, M., Zheng, H., He, Y., Chen, M.-X., Tang, W., Yue, X., Huang, Y., Zhuang, L., et al. (2020). Gut dysbiosis induces the development of pre-eclampsia through bacterial translocation. Gut, gutjnl-2019-319101. https://doi.org/10.1136/gutjnl-2019-319101.
8. Wrzosek, L., Ciocan, D., Borentain, P., Spatz, M., Puchois, V., Hugot, C., Ferrere, G., Mayeur, C., Perlemuter, G., and Cassard, A.-M. (2018). Transplantation of human microbiota into conventional mice durably reshapes the gut microbiota. Scientific reports 8, 6854. https://doi.org/10.1038/s41598-018-25300-3.
9. Willis, K.A., Siefker, D.T., Aziz, M.M., White, C.T., Mussarat, N., Gomes, C.K., Bajwa, A., Pierre, J.F., Cormier, S.A., and Talati, A.J. (2019). Perinatal maternal antibiotic exposure augments lung injury in offspring in experimental bronchopulmonary dysplasia. American Journal of Physiology - Lung Cellular and Molecular Physiology 3, 21. https://doi.org/10.1152/ajplung.00561.2018.
10. Nardiello, C., Mižíková, I., Silva, D.M., Ruiz-Camp, J., Mayer, K., Vadász, I., Herold, S., Seeger, W., and Morty, R.E. (2017). Standardisation of oxygen exposure in the development of mouse models for bronchopulmonary dysplasia. Disease models & mechanisms 10, 185–196. https://doi.org/10.1242/dmm.027086.
11. Ezz-Eldin, Z.M., Hamid, T.A.A., Youssef, M.R.L., and Nabil, H.E.-D. (2015). Clinical Risk Index for Babies (CRIB II) Scoring System in Prediction of Mortality in Premature Babies. J Clin Diagnostic Res 9, SC08-11. https://doi.org/10.7860/jcdr/2015/12248.6012.
12. Baker, J.M., Hinkle, K.J., McDonald, R.A., Brown, C.A., Falkowski, N.R., Huffnagle, G.B., and Dickson, R.P. (2021). Whole lung tissue is the preferred sampling method for amplicon-based characterization of murine lung microbiota. Microbiome 9, 99. https://doi.org/10.1186/s40168-021-01055-4.
13. Pierre, J.F., Phillips, G.J., Chandra, L.C., Rendina, D.N., Thomas-Gosain, N.F., Lubach, G.R., Lyte, M., Coe, C.L., and Gosain, A. (2021). Lyticase Facilitates Mycobiome Resolution Without Disrupting Microbiome Fidelity in Primates. J Surg Res *267*, 336–341. https://doi.org/10.1016/j.jss.2021.06.023.
14. Bolyen, E., Rideout, J.R., Dillon, M.R., Bokulich, N.A., Abnet, C.C., Al-Ghalith, G.A., Alexander, H., Alm, E.J., Arumugam, M., Asnicar, F., et al. (2019). Reproducible,

interactive, scalable and extensible microbiome data science using QIIME 2. Nat Biotechnol 37, 852–857. https://doi.org/10.1038/s41587-019-0209-9.
15. Callahan, B.J., McMurdie, P.J., Rosen, M.J., Han, A.W., Johnson, A.J.A., and Holmes, S.P. (2016). DADA2: High-resolution sample inference from Illumina amplicon data. Nature methods 13, 581–583. https://doi.org/10.1038/nmeth.3869.
16. Smirnova, E., Huzurbazar, S., and Jafari, F. (2018). PERFect: PERmutation Filtering test for microbiome data. Biostatistics 20, 615–631. https://doi.org/10.1093/biostatistics/kxy020.
17. Wang, W., Yan, T., Guo, W., Niu, J., Zhao, Z., Sun, K., Zhang, H., Yu, Y., and Ren, T. (2021). Constitutive GLI1 expression in chondrosarcoma is regulated by major vault protein via mTOR/S6K1 signaling cascade. Cell Death Differ 28, 2221–2237. https://doi.org/10.1038/s41418-021-00749-4.
18. Nicola, T., Ambalavanan, N., Zhang, W., James, M.L., Rehan, V., Halloran, B., Olave, N., Bulger, A., Oparil, S., and Chen, Y.-F. (2011). Hypoxia-induced inhibition of lung development is attenuated by the peroxisome proliferator-activated receptor-γ agonist rosiglitazone. American Journal of Physiology - Lung Cellular and Molecular Physiology *301*, L125-34. https://doi.org/10.1152/ajplung.00074.2011.
19. Nicola, T., Hagood, J.S., James, M.L., MacEwen, M.W., Williams, T.A., Hewitt, M.M., Schwiebert, L., Bulger, A., Oparil, S., Chen, Y.-F., et al. (2009). Loss of Thy-1 inhibits alveolar development in the newborn mouse lung. Am J Physiol-lung C 296, L738–L750. https://doi.org/10.1152/ajplung.90603.2008.
20. Tiew, P.Y., Dicker, A.J., Keir, H.R., Poh, M.E., Pang, S.L., Aogáin, M.M., Chua, B.Q.Y., Tan, J.L., Xu, H., Koh, M.S., et al. (2021). A high-risk airway mycobiome is associated with frequent exacerbation and mortality in COPD. Eur Respir J 57, 2002050. https://doi.org/10.1183/13993003.02050-2020.
21. Ali, N.A.B.M., Aogáin, M.M., Morales, R.F., Tiew, P.Y., and Chotirmall, S.H. (2019). Optimisation and Benchmarking of Targeted Amplicon Sequencing for Mycobiome Analysis of Respiratory Specimens. Int J Mol Sci 20, 4991. https://doi.org/10.3390/ijms20204991.
22. Jilling, T., Ren, C., Yee, A., Aggarwal, S., Halloran, B., Ambalavanan, N., and Matalon, S. (2018). Exposure of neonatal mice to bromine impairs their alveolar development and lung function. American Journal of Physiology - Lung Cellular and Molecular Physiology *314*, L137–L143. https://doi.org/10.1152/ajplung.00315.2017.